Journal of
MECHANICAL and ENERGY
ENGINEERING

ISSN: 2544-0780 | e-ISSN: 2544-1671
Vol. 5(45) | No. 2 | June 2021 | pp. 113-122
DOI: 10.30464/jmee.2021.5.2.113

INVESTIGATION OF NON-IMAGING FRESNEL LENS PROTOTYPING WITH DIFFERENT MANUFACTURING METHODS FOR SOLAR ENERGY APPLICATION

Ai Jiang SEXTON[1], Hassan QANDIL[1, 2], Mohammad ABDALLAH[3], Weihuan ZHAO[1*]

[1] Department of Mechanical Engineering, University of North Texas, USA
[2] Applied Science Private University, Amman, Jordan
[3] Al Hussein Technical University, Amman, Jordan
[1*] Faculty of Mechanical Engineering, Department of Mechanical Engineering, University of North Texas, 3940 North Elm Street, Denton, Texas 76207, USA, e-mail: weihuan.zhao@unt.edu

(Received 6 April 2021, Accepted 3 May 2021)

Abstract: Non-imaging Fresnel lenses have been playing an important role in improving the efficiency of solar energy systems. Many researchers have been developing novel designs of Fresnel lenses to enhance the concentrator performance. To bring the complex design of the Fresnel lens from a conceptual theory to a real-life application while maintaining its efficiency, it is critical to find the optimum manufacturing method that achieves the best quality fabrication at a low cost in the lab scale. This work will systematically investigate four advanced manufacturing methods for their lens-making capabilities, including pressure casting, hot embossing, 3D printing, and CNC machining. Six Fresnel lenses were fabricated by the four methods, which were tested in the lab by a solar simulator and a solar cell to demonstrate their performances. The CNC machining provides the best quality lab-scale Fresnel lens that enhances the solar cell efficiency by 118.3%. 3D printing and hot embossing methods are also promising for the fabrication of good performance lenses: increasing the solar cell efficiency by 40-70%. However, the 3D printed lens has the issue of material degradation over the long term. Although pressure casting is the easiest manufacturing method, the performance of the lens fabricated was the lowest.

Keywords: non-imaging Fresnel lens, CNC machining, 3D printing, hot embossing, pressure casting, solar energy

1. INTRODUCTION

Even with being invented back the 1800s, Fresnel lenses, both imaging and non-imaging types, continue to advance the efficiency of current optical technologies. Non-imaging Fresnel lenses can have a higher optical efficiency than the imaging type, with higher concentration ratios, shorter focal lengths, controllable focal flux distribution and larger acceptance angles [1-6]. This type of lens is typically made of low-cost acrylic polymers, much thinner and lighter compared to traditional convex and concave lenses, and show promising results in the field of concentrated solar power compared to parabolic troughs [1,2,6]. Applications of the non-imaging lens include enhanced illumination and light collimation systems, concentrated photovoltaics (CPV), concentrated so-lar power (CSP), solar cooking and other thermal applications [1-6]. For instance, Leutz *et al*. investigated how employing Fresnel lens-based solar concentration could justify well-distributed solar irradiation over the photovoltaic (PV) panel without tracking operation [7]. Most recently, Verma *et al.* explained how the monocrystalline PV efficiency increased when in-stalling Fresnel lenses in a photovoltaic/thermal (PV/T) system [6].

However, the lab-scale prototyping costs of the Fresnel lenses can be considerably expensive, mainly due to the high capital required for making a mould of

prismatic grooves [1]. More novel ideas of the Fresnel lenses like the double total internal reflection (DTIR) by Zhuang and Yu [5] and the optimized design for tracking error mitigation by Qandil *et al*. [8] shed light on the importance of lower cost manufacturing methods of the Fresnel lens, especially in the proof-of-concept phase of the research.

Many publications described the use of injection moulding (IM) and injection compression moulding (ICM) in the mass production of optical elements, especially for manufacturing high precision lenses at micro/nano scales, with advantages of better nano surface finishing, higher geometrical replication fidelity and mass production capability. However, the use of IM for initial lens prototyping is extensively pricy [9-14].

Hot embossing is another method for high-precision Fresnel lens manufacturing. Lu *et al*. used hot embossing to fabricate dielectric Fresnel zone plates (DFZPs) as micro-lenses on tips of plastic optical fibers (POFs). DFZPs were made on a glass substrate by photolithography with an ink printed lithography mask, and then used as a template for hot embossing on the tip of a polymethyl-methacrylate (PMMA) POF [15]. It was observed that the DFZP on the POF tip was able to achieve light focusing while maintaining high light intensity based on optical measurements [15]. Pham *et al*. developed a novel linear Fresnel lens with two groove surfaces placed perpendicular to each other [16]. Due to the special asymmetric geometry, hot embossing was considered as a potential method to manufacture their proposed linear Fresnel lens [16].

3D printing method was also explored for fabricating complex Fresnel lenses with reduced costs. Shrotri *et al*. used an ultraviolet-curing-based stereolithography (UV-SLA) 3D printer combined with lacquering as a post-processing method to manufacture a Fresnel lens [17]. It was found that the fabricated lens could achieve the lowest attenuation (losses) at 635 nm wavelength in the red visible light to infrared wavelength range [17].

Most recently, Tan *et al*. developed the Direct Diamond Shaping method to enable the Ultra-Precision Machining (UPM) technology to achieve a combination of linear and rotary features, providing highly accurate geometric and surface finish for the Fresnel lens, micro-channel fabrications [18].

Novel designs of Fresnel lenses usually require expensive manufacturing techniques from the perspective of initial prototyping. Advancing and extending from the current studies, this paper aims to explore different lab-scale Fresnel lens manufacturing methods (including a new advanced CNC machining method for this application) that enable complex geometry fabrication in an accurate manner. This is the first work to systematically investigate and compare various in-lab manufacturing methods for the Fresnel lens (with novel design and complex configuration) fabrication to explore their capabilities.

2. MATERIALS AND METHODS

2.1. Manufacturing methods

Lab-scale fabrication of the Fresnel lens has the key objective of transforming a theoretically-optimized design into a real prototype, which can be tested to verify the original simulations.

In this work, four fabrication methods were selected: pressure casting, hot embossing, 3D printing, and CNC machining. CNC machining is uniquely proposed here, and it has barely been studied before for Fresnel lens fabrication. All the methods were compared for the finished lenses performance.

2.1.1. Pressure casting

Being an extensively researched lab-scale method, pressure casting is a relatively matured technique for Fresnel lens fabrication. In this process, the piece was 3D printed first via an inverted stereolithography (SLA) technique, then carefully post-processed with sanding and heating to melt out surface impurities. The piece does not necessarily have to be transparent but it needs a very detailed and smooth surface finish to create an open-face silicone mold, as displayed in Fig. 1(a). It was using platinum-cure silicone rather than tin-cure to prevent post-cast fogging. Moreover, the silicone liquid mixed was vacuum degassed to remove air trapped during mixing or pouring that could jeopardize the mold's surface finish. After that, the silicone was set at room temperature for 6-8 hours for solidification and demolding.

Clear self-setting acrylic was vacuum degassed, then poured into a silicone mold and pressurized inside a pressure chamber at 40-50 psi for 24 hours. The finished lens in Fig. 1(b) was fine-polished by a diamond-based compound to boost the optical clarity. The final lens was 120-mm-diameter spot Fresnel lens with the focal ratio (f-number) of 1, a thickness of 5 mm (overall thickness), and 15 grooves of an equal 4-mm width (the same groove width was applied for all the lab-fabricated spot lenses explained below in this study). The total fabrication time for the lens using the pressure casting method (including silicone mold fabrication) was 36 hours.

While this method can be lower in cost and easier in manufacturing, it also consists of multiple sub-processes (for the piece, the mold and the lens) that could complicate the quality control and increase the chances of having defects like air bubbles. The material used to produce the lens, i.e. self-setting acrylic, is also sensitive to ultraviolet (UV) light, which causes faster degradation of the lens quality.

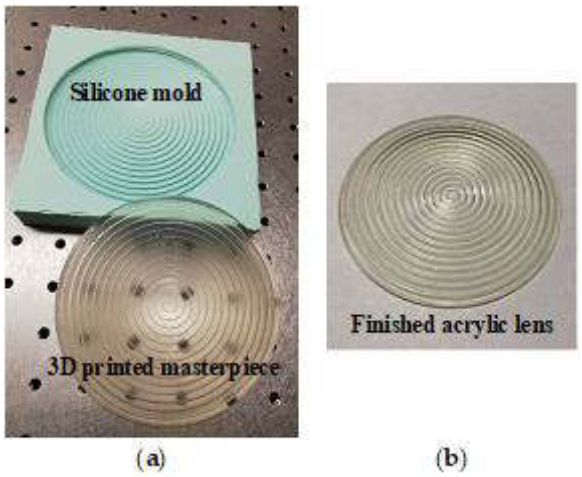

Fig. 1. Sub-processes for pressure casting method: (a) An open-face silicone mold created by a piece; (b) Finished acrylic lens through the silicone mold

2.1.2. Hot embossing

This method can be cost competitive for in-lab manufacturing [19-20]. A steel master mold is fabricated by wire-cut electrical discharge machining (Wire-EDM), as shown in Fig. 2(a). The wire-EDM machine used for this work is Mitsubishi® FX10. The steel master mold was cut with a 0.25-mm-diameter wire fed at the rate of 12.5 mm (0.5inch) per minute. The wire diameter and its spooling speed could have an effect on the surface finish of the mold. It is noted that wire-EDM can only be used for linear-lens molds. Spot-lens molds can be fabricated by CNC machining. The finished master mold has smooth sur-face finish of approximately 0.375-0.5 μm (15-20 micro-inch) *Ra* (average roughness). It was then heated in a hydraulic press machine to about 193°C (380°F); once the temperature has stabilized, the PMMA acrylic sheet is compressed into the master mould at 10-15 tons of pressure and constant temperature until its lower surface is shaped in the groove geometry (Fig. 2(b)). Both the mold and the sheet formed are then cooled to about 66 – 82°C (150 – 180°F) at a constant pressure of 10 tons. The acrylic piece formed is then naturally cooled, removed from the mold, and cleaned. The excess sides are laser-cut. A 90 mm × 120 mm linear lens with 5 mm overall thickness, 38 grooves of an equal 3-mm width and 240 mm focal length, shown in Fig. 2(c), was made using this method. The overall fabrication time for the lens using the hot embossing method (including wire-EDM machining for a master mold) was 10 hours.

The well-designed master mould is economically reasonable for frequent fabrication, and it provides flexibility to try different lens materials. Nevertheless, the process involves the use of multiple heavy-duty equipment, so the upfront setup cost may be high. Also, similar to pressure casting, the master mould for hot embossing is lens-specific, which imposes a prototyping limitation [21]. In addition, when multiple processes, parts, and procedures are involved, the final product will always have risks of defects.

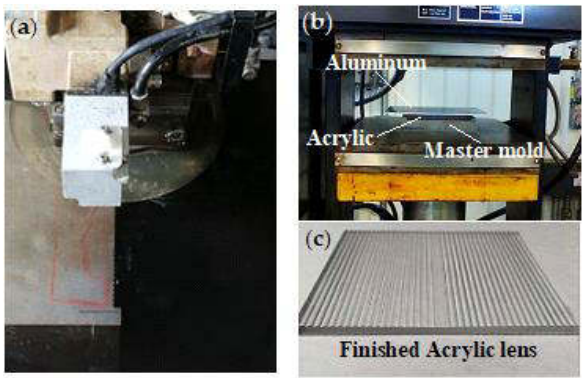

Fig. 2. Sub-processes for hot embossing method: (a) Wire-EDM cutting for a steel master mold; (b) Compressing a PMMA acrylic sheet into the master mold at elevated temperature and pressure; (c) Hot-embossed finished acrylic lens

2.1.3. 3D printing

An inverted SLA 3D printer by Formlabs®, shown in Fig. 3(a), was used with a clear UV-curable resin fed from a bottom tank. The printer has a laser spot size of 140 microns, Z resolution (the layer thickness) of 25-300 microns, and XY resolution of 2.8 microns.

The photosensitive resin is solidified, layer by layer, using UV light until the full lens geometry is created. Once the support structure is removed manually, post-processing of the lens would include polishing the flat surface, clear spray paint coating up to 4 layers, and finally dipping in a de-gassed clear resin for enhanced transparency.

The completed lens in Fig. 3(b) had a comparably decent surface finish with high dimensional accuracy of prisms and good clarity. It was a 5-mm-thick (overall thickness) spot-lens with 120 mm diameter and focal length, and 15 prism grooves. This method provides ease and low cost of prototyping. The total fabrication time was approximately 20 hours.

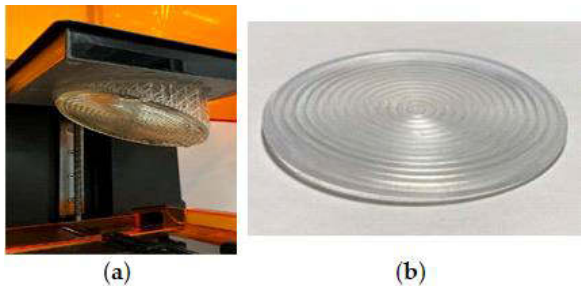

Fig. 3. 3D printing method for Fresnel lens manufacturing: (a) Inverted 3D printing of lens; (b) Finished 3D-printed lens

However, when used in solar energy systems, the worst disadvantage is associated with the lens material. Since the curable resin is sensitive to UV light, a fast degradation of transparency can be

expected when exposed to sunlight for long periods of time. Surface fogging could also be noticed if the post-processing was not done rapidly and accurately.

2.1.4. CNC machining

Computer numerical control (CNC) machining is a unique manufacturing method we proposed for this application, which has not been utilized to fabricate Fresnel lenses for solar concentration. In this work, a 3-axis DMG Mori Seiki DuraVertical 5060 CNC milling was applied to fabricate the lenses, as seen in Fig. 4.

The lens's surface finish and clarity depend solely on the machining procedure and the tool selection. PMMA acrylic sheets with two different thicknesses were selected. The cutting tool, a flute solid-carbide ball-end mill, was set to move circumferentially. The depth of the cut was set to 0.06" with a 0.04" tool diameter (for deep grooves near the spot lens edge), 0.03" with 0.02" and then 0.01" tool diameter (for shallow grooves close to the center), respectively. Two spot lenses were produced: one was a 5 mm-thick (overall thickness) lens with 120 mm diameter and focal length, and 15 prism grooves; the other was a 10 mm-thick (overall thickness) lens with 104 mm diameter, 120 mm focal length, and 13 prism grooves.

Each lens required about 5.75 hours of machine and labor work, and both had relatively good clarity despite the machining marks that were observed on the groove-side. Factors such as the feed rate and cutting strategy can have a huge impact on the lens quality. As observed in our preceding trials for CNC lenses, higher feed rates can cause more observable surface marks and lower surface finish, while cutting outwards (center-to-edge) had smoother finish than cutting inwards (edge-to-center).

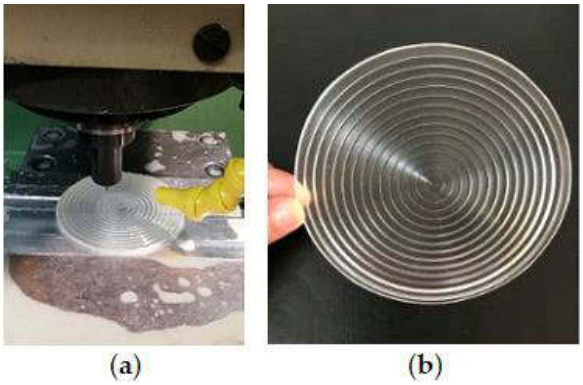

Fig. 4. CNC machining process: (a) Open-face CNC machining of lens; (b) Finished CNC-machined acrylic lens (the 5-mm-thick lens)

The light transmission efficiency for the acrylic material used in hot embossing and CNC machining methods was greater than 92% [22]. The epoxy resin for pressure casted lenses and UV curable clear resin for 3D printed lenses had a slightly lower transmission efficiency, but still greater than 90% [23]. Nevertheless, the actual light transmission of the lens could be further reduced due to the manufacturing procedure.

2.2. Experimental methodologies

The Fresnel lenses fabricated from the aforementioned manufacturing methods were tested in the lab through a solar simulator and dye-sensitized solar cell (DSSC). The principle of testing is to measure the current-voltage characteristic curve (I-V curve) generated from the solar cell when it is illuminated by the solar simulator. The tests were conducted in the Chemistry Lab at University of North Texas (UNT) using a solar cell spectral response/QE/IPCE measurement system. The experimental set-up is shown in Fig. 6. The solar simulator generates the input power of one sun with the standard reference spectra of Air Mass (AM1.5) solar spectrum. This solar-simulated irradiation supplies an integrated lighting intensity of 100 mW/cm^2, which provides a sunlight spot size of 57 mm diameter and a working distance of 450 mm from the exit port. The solar cells tested were N719 DSSC [24] fabricated in the chemistry lab at UNT. The solar cell was connected to a multimeter for voltage and current readings. The multimeter has the measurement error of ±0.14%. To obtain precise and stable sunlight intensity for testing, a solar reference cell made of monocrystalline silicon was used to calibrate the height of the support clamp that positions the solar cell. The clamp height was set fixed when the meter read a current of 49.8 ± 0.7 mA from the calibration cell circuit under simulated solar light. After calibration, the distance between the cell and the solar simulator was fixed at 450 mm for this study. The calibration cell was then replaced with the N719 cell as a testing base. The position of the N719 cell was fixed at the clamp while the position of the lens was adjusted to reach the highest possible voltage reading on the multimeter. All the data obtained was collected by a computer with the LabTracer system software.

The Fresnel lens performance test is based on the solar energy conversion efficiency of the solar cell, which is determined by the ratio of the power output converted by the solar cell and the power input that the solar cell received from the solar simulator. Through calculating the energy conversion efficiency, it may explore the enhancement of the solar cell efficiency by using the lens.

Figure 5 shows the relationship between the output current and the power of the circuit, used in calculating the energy conversion efficiency [25]. It should be noted that a passive device that requires power supply will have an I-V curve passing through quadrant I or III, while an active device that can generate electrical power will result in an I-V curve crossing quadrant II or IV in the Cartesian coordinates.

When the solar cell is exposed to sunlight, the cell generates power, which is fed to an active device. Therefore, the actual I-V curve of the solar cell will be in quadrant IV (see the testing result Fig. 7 in the RESULTS AND DISCUSSION section). Here, Fig. 5 provides a diagram that shows the absolute values of current for the energy conversion efficiency calculation purpose.

While calculating the conversion efficiency, current density J (current per unit area of solar cell) is normally used instead of current I to eliminate the effect of the cell size on the resulting current. Several important intersections provide the basis to determine the performance of the cell. The intersection point of the I-V (J-V) curve and y-axis, point J_{SC}, is the short circuit current flowing through the cell when the voltage across is zero. This is also the maximum current that a solar cell can possibly generate. When the net current flowing through the cell is zero, the open circuit voltage: V_{OC} is observed. This is the maximum voltage available from the solar cell. V_{MP} and J_{MP} are the voltage and current at the maximum power output P_{MP}. Fill factor (FF) is defined as [25]:

$$FF = \frac{P_{MP}}{V_{OC} \times J_{SC}} = \frac{V_{MP} \times J_{MP}}{V_{OC} \times J_{SC}}. \quad (1)$$

Hence, the incident photon-to-electron conversion efficiency η of the solar cell can be calculated by [25]:

$$\eta = \frac{P_{out}}{P_{in}} = \frac{FF \times J_{SC} \times V_{OC}}{P_{in}} \times 100\%. \quad (2)$$

where P_{out} is the power output generated by the cell; P_{in} is the power input that the cell receives from the` solar simulator (i.e., 100 mW/cm^2). The J_{SC}, V_{OC}, J_{MP} and V_{MP} were measured in the experiment to calculate the efficiency.

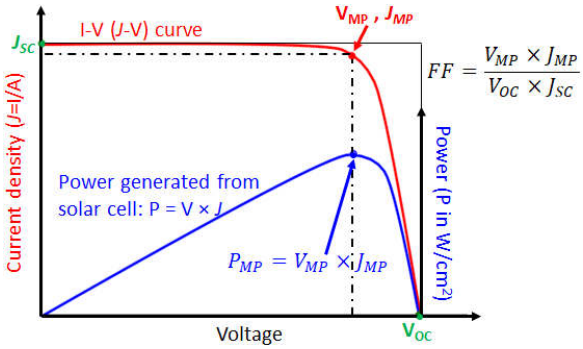

Fig. 5. I-V (J-V) curve of solar cell (cell output current density and power) [25]

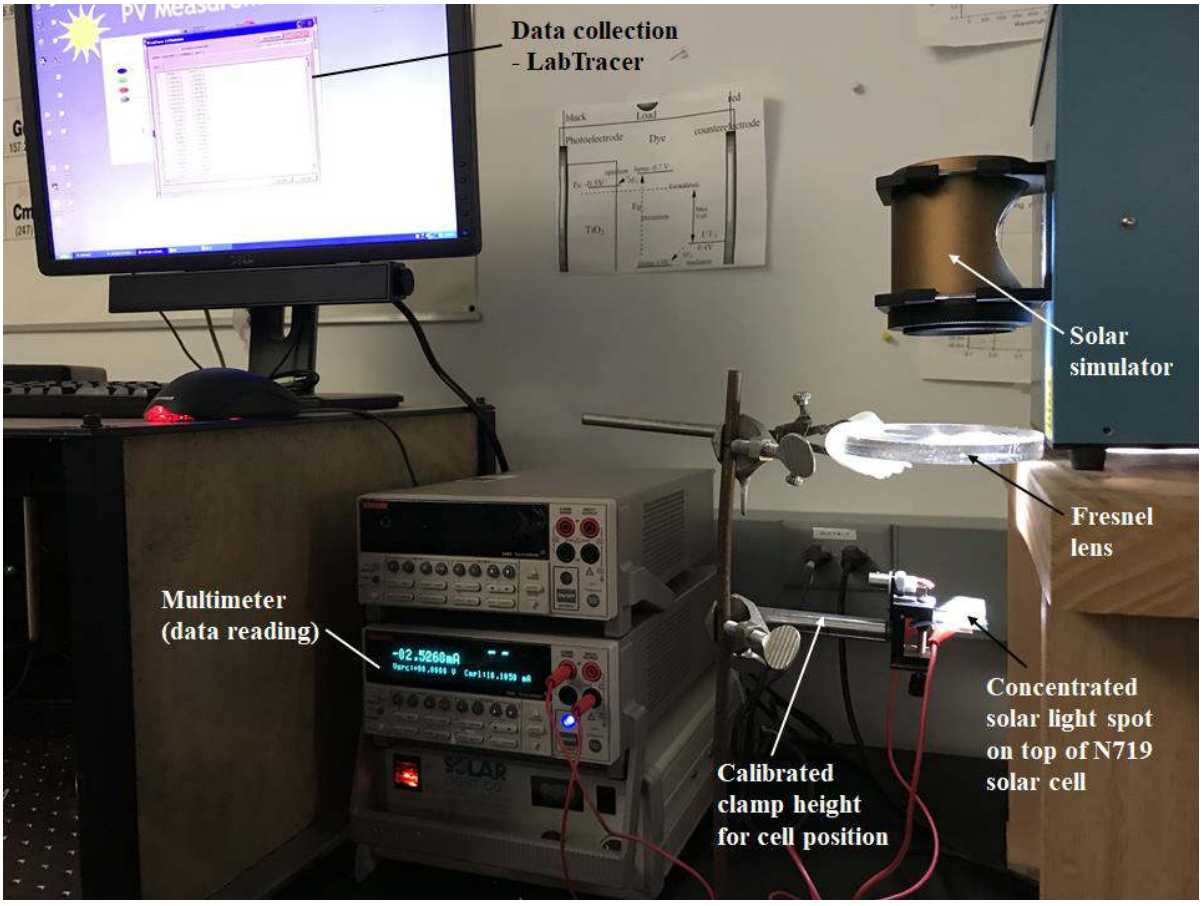

Fig. 6. Experimental set-up including a solar simulator, Fresnel lens, solar cell, multimeter, and workstation for data collection and recording

The FF value is affected by the voltage as well as many other factors, such as the type of the cell, the cell material and the temperature on the cell surface. The Fresnel lens can increase the cell surface temperature, resulting in an enhancement of the FF value and the efficiency of the solar cell.

3. RESULTS AND DISCUSSION

Six Fresnel lenses fabricated using the aforementioned four manufacturing methods were tested in this study. Table 1 summarizes the detailed specifications of each lens. The lenses' performances were compared considering the factors of the manufacturing methods, the corresponding required materials and product geometries associated with the fabrication process. Nevertheless, all the lenses had the same groove configuration.

Each lens was repeatedly tested for three times. It was found that the readings were consistent between each time. Table 2 displays the testing results for the solar cell (i.e., J_{MP}, J_{SC}, V_{OC}, FF and η) under concentrated solar light generated from each lens. The solar cell used (lab-fabricated N719 DSSC) is rated for 0.5V with an active area of 0.36 cm^2. It was tested with a base efficiency of 1.28%. After installing the Fresnel lenses, the solar cell efficiency was enhanced due to the increased surface temperature. Figure 7 shows the I-V (*J*-V) curves of the solar cell before and after using the fabricated Fresnel lenses.

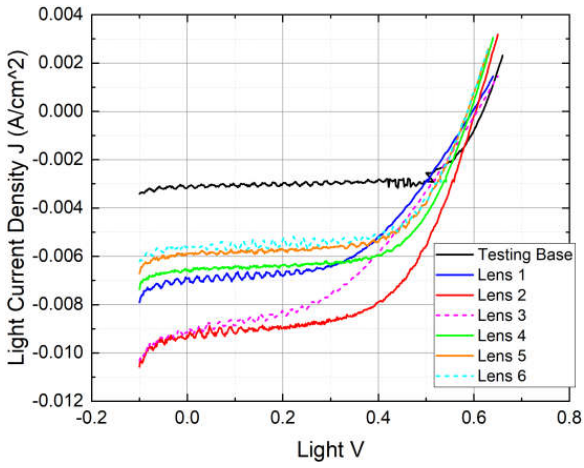

Fig. 7. I-V (*J*-V) curves of the solar cell before and after applying Fresnel lenses

Compared to the base, the CNC milled lens (with an overall thickness of 5mm) produced an efficiency increase of 118.3% and was the best performer among all the lab-fabricated Fresnel lenses. Its outstanding performance increased the current density at the maximum power from 2.6 mA/cm^2 to 5.6 mA/cm^2, short circuit current density from 3.1 mA/cm^2 to 9.4 mA/cm^2 and, consequently, the overall efficiency from 1.28% to 2.78%. However, with the lens base made two times thicker, the enhancement of photon-to-electron conversion efficiency dropped to one-fourth as illustrated in Table 2.

The CNC milled lens with a thicker 10-mm base produced current density with the maximum power of 3.3 mA/cm^2 (versus 5.6 mA/cm^2 for thin base), the open circuit current density of 9.0 mA/cm^2 (versus 9.4 mA/cm^2 for the thin base). The overall efficiency enhancement achieved by the thick base lens was 28.6% (versus 118.3% by the thin base lens). Two I-V (*J*-V) curves for the CNC milled lenses (lens 2 and 3) have about the same starting point at voltage 0, but start to diverge and deviate away to different paths at voltage 0.1 V as shown in Fig. 7. Beyond 0.3 V, the difference between the two curves reaches the farthest apart. Although the thick base lens provides an easier fabrication approach for the CNC milling machine due to better holding of the workpiece in place, the drawback is a lower efficiency caused by the unnecessary extra material used.

The next competitor is the 3D printed spot lens (Lens 4) that offers a 67.4% increase in the solar cell efficiency. With almost doubled short-circuit current (J_{SC}), the overall efficiency increased from 1.28% (base) to 2.13%. However, due to the UV-curable resin (the material required for the 3D printing device), the material degradation over time will need to be taken into consideration when implementing the 3D printed lens into real-world applications.

Following are the hot-embossed linear lenses, over 40% efficiency increase was achieved for both naturally-cooled (slow) and fan-cooled (fast) lenses. The fast-cooled lens (Lens 5) performed slightly better than the slow-cooled lens (Lens 6) in testing. The current density at the maximum power increased from 2.6 mA/cm^2 (base) to 3.8 mA/cm^2 for the fast-cooled ones and 3.7 mA/cm^2 for the slow-cooled ones; the short circuit current density increased from 3.1 mA/cm^2 (the base) to 5.9 mA/cm^2 for the fast-cooled ones and 3.6 mA/cm^2 for the slow-cooled ones. The open circuit voltage dropped by approximately the same amount for both lenses (from 0.62V (the base) to 0.59 V). Hence, the overall efficiencies were 1.91% for the fast-cooled and 1.84% for the slow-cooled lens (Table 2). The two I-V (*J*-V) characteristic curves for the fast-cooled and slow-cooled hot-embossed lenses are closely laid out in Fig. 7. It starts to overlap with the voltage approaching 0.45 V and beyond. Moreover, the geometry of the hot-embossed lenses was different from others, i.e., linear lens versus spot lens, due to the geometry limitation of the hot embossing method in our lab. The wire-EDM cutting could only make linear lens-based master mold. The difference in the geometry could also affect the solar concentration performances of hot-embossed Fresnel lenses.

Tab. 1. Lens specifications

	Manufact-uring methods	Lens dimensions	Focal length (mm)	Overall thickness (mm)	Material	Groove pitch (mm)	Refractive index	Light transmittance* (%)
Lens 1	Pressure casting	Spot lens, 120mm (D)	120	5	Clear epoxy resin	4	1.5-1.65 [23]	>90
Lens 2	CNC milling	Spot lens, 120mm (D)	120	5	PMMA	4	1.48-1.50 [22]	>92
Lens 3	CNC milling	Spot lens, 104mm (D)	120	10	PMMA	4	1.48-1.50 [22]	>92
Lens 4	3D printing	Spot lens, 120mm (D)	120	5	UV-curable clear resin	4	1.41-1.59 [23]	>90
Lens 5	Hot embossing, fast cooling	Linear lens, 90mm(W)×120mm(L)	240	5	PMMA	3	1.48-1.50 [22]	>92
Lens 6	Hot embossing, slow cooling	Linear lens, 90mm(W)×120mm(L)	240	5	PMMA	3	1.48-1.50 [22]	>92

* Light transmittance data is based on the raw materials. The light transmissions of the final lenses can be further reduced due to the manufacturing procedure.

Tab. 2. Solar cell testing results for various Fresnel lenses fabricated by different manufacturing methods

Lens	Description	V_{MP} (V)	J_{MP} (A/cm^2)	J_{SC} (A/cm^2)	V_{OC} (V)	FF	η	η increase
No lens (base)	Testing base N719 solar cell, without using lens	0.5001	0.0026	0.0031	0.6200	0.6549	1.28%	---
Lens 1	Pressure casting	0.5009	0.0029	0.0069	0.5974	0.3466	1.43%	12.4%
Lens 2	CNC milling, 120mm DIA, 5mm thick	0.5016	0.0056	0.0094	0.6048	0.4922	2.78%	118.3%
Lens 3	CNC milling, 104mm DIA, 10mm thick	0.5015	0.0033	0.0090	0.6086	0.2997	1.64%	28.6%
Lens 4	3D printed	0.5009	0.0043	0.0066	0.5937	0.5479	2.13%	67.4%
Lens 5	Hot embossing, fast cooling	0.5000	0.0038	0.0059	0.5879	0.5516	1.91%	49.8%
Lens 6	Hot embossing, slow cooling	0.5001	0.0037	0.0056	0.5878	0.5546	1.84%	43.9%

The least competitive lens is the pressure cast spot lens (Lens 1). The current density at the maximum power was boosted from 2.6 mA/cm^2 (base) to 2.9 mA/cm^2. The short circuit current density was increased from 3.1 mA/cm^2 to 6.9 mA/cm^2 while the open circuit voltage decreased from 0.62V to 0.60V. These parameters contribute to an overall efficiency of 1.43%, which was only increased by 12.4% compared to the base (without lens).

4. CONCLUSIONS

From among all of the in-lab manufacturing methods studied in this paper, the method of using CNC milling machines has proven to be the best approach of prototyping complex-geometry Fresnel lens concentrators. The method provided better flexibility for fabricating spot or linear lenses, potentially even dome-shaped lenses if setup properly. The time requirement of machine and labor work is also the shortest among the four lab-scale manufacturing methods. The base of the lens could be made thinner for better lens performance. The use of a vast variety of cutting tools, adding more machining axes, and adjusting the different machining settings can all be further explored and implemented to achieve better results. The method also showed great adaptability to working with different types of materials. In addition, the lenses showed excellent clarity and transparency as well as great stability and reliability in performance without any degradation detected over a 10-month period. The CNC milling method has a minor effect on the lens base, such as scratches and marks. Even though chatter marks were the result of the fabrication process on each edge of lens grooves, no evidence was found that the chatter marks were affecting the lens performance.

The cost-effective and rapid prototyped 3D printed spot lens also showed good solar concentration performance in the test. Nevertheless, the lens has shown a mild level of material degradation over a 10-month period; the color of the lens was slightly changed with time. Hence, the lens performance deterioration can be predicted when used in field for a long-term duration. When made using a hot embossing method, the finished lenses also have good clarity and transparency. It was found that a fast-

cooled lens using a fan offers a better performance. Hence, the cooling time and procedure can further be studied in the future to identify the optimum cooling rate for achieving better solar concentration performance. Pressure casting, as the most commonly used and extensively studied fabrication method, was found to be on the bottom of the performance list. Ease of mass production with low fabrication costs may offset the low efficiency; but for prototyping purposes it was not effective. The decision of selecting a suitable method for lab-scale fabrication can be made upon atrade-off between the cost and the performance.

This work has demonstrated the capability and advance of the CNC machining method for complex-geometry, high-accuracy manufacturing. It opens a new avenue in low-cost lab-scale Fresnel lens concentrator prototyping although heavy CNC equipment may impose a much higher upfront fabrication investment.

Acknowledgements

This research was supported by Solar Solution DC LLC. The Authors would like to thank Dr. Francis D'Souza and his Ph.D. student, Ajyal Alsaleh, from the Chemistry Department at UNT for sharing their lab equipment and providing the knowledge of experimental measurements in this research work.

Nomenclature

Symbols

A – area of solar cell, cm^2
FF – fill factor, –
I – current, A or mA
J – current density, A/cm^2 or mA/cm^2
J_{MP} – current density at maximum power output, A/cm^2 or mA/cm^2
J_{SC} – current density when short circuit current occurs, A/cm^2 or mA/cm^2
P_{in} – power input, W/cm^2 or mW/cm^2
P_{MP} – maximum power output, W/cm^2 or mW/cm^2
P_{out} – power output, W/cm^2 or mW/cm^2
Ra – arithmetical mean deviation of roughness, μm
V – voltage, V
V_{MP} – voltage at maximum power output, V
V_{OC} – open circuit voltage, V

Greek letters

η – incident photon-to-electron conversion efficiency,

Acronyms

CNC – Computer Numerical Control
CPV – Concentrated Photovoltaics
CSP – Concentrated Solar Power
DFZP – Dielectric Fresnel Zone Plate
DSSC – Dye-Sensitized Solar Cell
DTIR – Double Total Internal Reflection
ICM – Injection Compression Moulding
IM – Injection Moulding
PMMA – Polymethyl-methacrylate
POF – Plastic Optical Fiber
PV – Photovoltaics
PV/T – Photovoltaic/Thermal
Ra – Average Roughness
SLA – Stereolithography
UNT – University of North Texas
UPM – Ultra-Precision Machining
UV – Ultraviolet
UV-SLA –Ultraviolet-Curing-Based Stereolithography

References

1. Chaves J. (2016). *Introduction to Nonimaging Optics*. 2nd edition. CRC Press, Taylor & Francis Group, Boca Raton, Florida, USA.
2. Xie W.T., Dai Y.J., Wang R.Z., Sumathy K. (2011). Concentrated solar energy applications using Fresnel lenses: A review. *Renewable and Sustainable Energy Reviews,* Vol. 15, No. 6, pp. 2588–2606.
3. Akisawa A., Sato T., Miyazaki T., Kashiwagi T., Hiramatsu M. (2007). High concentration non-imaging Fresnel lens design with flat upper surface. In: Proceedings Volume 6649, High and Low Concentration for Solar Electric Applications II, 66490F, San Diego, California, USA.
4. Qandil H., Wang S., Zhao W. (2019). Application-based design of the Fresnel-lens solar concentrator. *Renewables: Wind, Water, and Solar,* Vol. 6, 3.
5. Zhuang Z., Yu F. (2014). Optimization design of hybrid Fresnel-based concentrator for generating uniformity irradiance with the broad solar spectrum. *Optics & Laser Technology,* Vol. 60, pp. 27–33.
6. Verma S., Verma A., Kumar V., Gangil B. (2021). Concentrated photovoltaic thermal systems using Fresnel lenses – A review. *Materials Today: Proceedings,* Vol. 44, No. 6, pp. 4256-4260.
7. Leutz R., Suzuki A., Akisawa A., Kashiwagi T. (1999). Design of a nonimaging Fresnel lens for solar concentrators. *Solar Energy,* Vol. 65, No. 6, pp. 379–387.
8. Qandil H., Wang S., Zhao W. (2019). Optimizing the Fresnel-Lens solar-concentrator design for tracking error mitigation in thermal applications, using a statistical algorithm. *Applied Solar Energy,* Vol. 55, pp. 106–112.
9. Kang S. (2004). Replication technology for micro/nano optical components. *Japanese Journal of Applied Physics,* Vol. 43, No. 8S, pp. 5706–5716.
10. Tosello G., Hansen H.N., Gasparin S., Albajez J.A., Esmoris J.I. (2012). Surface wear of TiN coated nickel tool during the injection moulding of polymer micro Fresnel lenses. *CIRP Annals - Manufacturing Technology,* Vol. 61, No. 1, pp. 535–538.
11. Sortino M., Totis G., Kuljanic E. (2014). Comparison of injection molding technologies for the production of micro-optical devices. *Procedia Engineering,* Vol. 69, pp. 1296–1305.
12. Lin C.-M. and Hsieh H.-K. (2017). Processing optimization of Fresnel lenses manufacturing in the injection molding considering birefringence effect. *Microsystem Technologies,* Vol. 23, pp. 5689–5695.
13. Loaldi D., Calaon M., Quagliotti D., Parenti P., Annoni M., Tosello G. (2018). Tolerance verification of precision injection moulded Fresnel lenses. *Procedia CIRP,* Vol. 75, pp. 137–142.
14. Loaldi D., Quagliotti D., Calaon M., Parenti P., Annoni M. and Tosello G. (2018). Manufacturing signatures of injection molding and injection compression molding for micro-structured polymer Fresnel lens production. *Micromachines,* Vol. 9, No. 12, 653.
15. Lu B.-R., Li J.-X., Guo H.-B., Gao C., Huq E., Qu X.-P., Chen Y., Liu R. (2011). Dielectric Fresnel zone plates on

optical fibers for micro-focusing applications. *Microelectronic Engineering,* Vol. 88, No. 8, pp. 2650-2652.
16. Pham T.T., Vu N.H. and Shin S. (2019). Novel design of primary optical elements based on a linear Fresnel lens for concentrator photovoltaic technology. *Energies,* Vol. 12, No. 7, 1209.
17. Shrotri A., Beyer M., Stübbe O. (2020). Manufacturing and analyzing of cost-efficient Fresnel lenses using stereolithography. In: Proceedings Volume 11349, 3D Printed Optics and Additive Photonic Manufacturing II, 113490N, SPIE Photonics Europe, Online Only.
18. Tan N.Y.J., Neo D.W.K., Zhang X., Liu K., Kumar A.S. (2021). Ultra-precision direct diamond shaping of functional micro features. *Journal of Manufacturing Processes,* Vol. 64, pp. 209-223.
19. Kujawa I., Kasztelanic R., Waluk P., Stępień R., Haraśny K., Pysz D., Klimczak M., Buczyński R. (2013). Fresnel lens fabrication for MidIR optics and fiber optic technique by using hot embossing process. In: Proceedings Volume 8698, Optical Fibers and Their Applications 2012, 869804, Krasnobrod, Poland.
20. Cirino G.A., Granado R.M., Mohammed-Brahim T. and Jasinevicius R.G. (2017). Assessment of replication fidelity of optical microstructures by hot embossing. *The International Journal of Advanced Manufacturing Technology,* Vol. 88, pp. 303–316.
21. Hot Embossing. MNX, MEMS & Nanotechnology Exchange. Available online: https://www.mems-exchange.org/catalog/hot_embossing/ (accessed on 11 October 2021).
22. I-Polymer – Typical Properties of Acrylic PMMA. Available online:
23. https://www.ipolymer.com/pdf/Acrylic.pdf (accessed on 11 October 2021).
24. MASTERBOND – Optically Clear Polymer Adhesives. Available online:
25. https://www.masterbond.com/properties/optically-clear-polymer-adhesives?matchtype=b&network=g&device=c&adposition=&keyword=optically%20clear%20adhesives&gclid=CjwKCAjwoc_8BRAcEiwAzJevtQ0VK7mrvG0G6r6lcG7_SolLvTaJJigS0GdFa2bzlczRBFlS5Ji8hhoCInEQAvD_BwE (accessed on 11 October 2021).
26. Zhang J., Yu C., Wang L., Li Y., Ren Y. and Shum K. (2014). Energy barrier at the N719-dye/$CsSnI_3$ interface for photogenerated holes in dye-sensitized solar cells. *Scientific Reports,* Vol. 4, 6954.
27. Honsberg C.B. and Bowden S.G. (2019). Chapter 4 – Solar Cell Operation. In: *Photovoltaics Education Website*. Available online: https://www.pveducation.org/ (accessed on 11 October 2021).

Biographical notes

Ai Jiang Sexton received her M.Sc. degree in Mechanical and Energy Engineering from the University of North Texas in 2020. She was the research team leader for the last two years of her bachelor's school years. The research project involved a failure modes analysis of spiral tube letdown heat exchangers sponsored by the Nuclear Power Institute, the Texas A&M Engineering Experiment Station. After graduating from the University of North Texas with a Bachelor's degree in Mechanical Engineer Technology in 2017, she joined Freese and Nichols, a consulting and engineering firm, working as a mechanical engineer. She completed her M.Sc. degree within 2.5 years while working full time as a mechanical engineer. She has been the leader for mechanical designs of multiple U.S. federal projects, Lockheed Martin facility upgrades, as well as water treatment projects. She is currently an assistant project manager of multiple projects involving both design and construction.

Hassan Qandil has been a researcher and a lecturer for the Department of Mechanical Engineering at the University of North Texas since 2019. He is also a certified energy manager who worked as a maintenance and operation engineer for international oilfield corporations in Jordan, Malaysia, UAE and India. Qandil received his Ph.D. degree in Mechanical and Energy Engineering from the University of North Texas in 2019, and both his B.Sc. and M.Sc. from the University of Jordan in 2009 and 2012, respectively. Qandil's research interests are in fields of solar energy optics, thermal management, energy harvesting and renewables.

Mohammad Abdallah received his BSE degree in Mechanical Engineering from Al Hussein Technical University in 2021. His industrial experience as a Mechanical Design Engineer in Jordan Light Vehicles Manufacturing (JLVM)-JODDB. His research interest covers designing and manufacturing UAVs' Turbojet Engine and Implementing Virtual Reality with Manufacturing Processes.

Weihuan Zhao receives her M.Sc. and Ph.D. degrees in Mechanical Engineering from Lehigh University in 2009 and 2013, respectively. After graduation from Lehigh University, she worked as a postdoctoral appointee at Argonne National Laboratory from 2013 to 2015. Since September 2015, she has been an assistant professor in the Department of Mechanical Engineering at the University of North Texas. Her scientific research interests focus on issues related with thermal management and thermal energy storage technologies, phase change materials (PCMs), high-temperature thermal-fluid experiments and solar energy technologies.